

# Photofragmentation of mass-selected $\text{ICl}^-(\text{CO}_2)_n$ cluster ions: Solvation effects on the structure and dynamics of the ionic chromophore

María E. Nadal, Paul D. Kleiber,<sup>a)</sup> and W. C. Lineberger<sup>b)</sup>  
*Department of Chemistry and Biochemistry and JILA, University of Colorado  
and National Institute of Standards and Technology, Boulder, Colorado 80309*

(Received 18 December 1995; accepted 1 April 1996)

Photofragmentation studies at 644 nm and 740 nm of  $\text{ICl}^-(\text{CO}_2)_n$  cluster ions ( $n=0-8$ ) have been carried out in a tandem time-of-flight mass spectrometer. Photodissociation of these cluster ions at a wavelength at which bare  $\text{ICl}^-$  produces only  $\text{I}^-$  results in the formation of three classes of fragment ions:  $\text{I}^-$ ,  $\text{Cl}^-$ , and  $\text{ICl}^-$  based clusters. The  $\text{I}^-$  based clusters correspond to the direct photoproduct in which a Cl atom has escaped the cluster ion. The  $\text{ICl}^-$  and  $\text{Cl}^-$  based clusters are a result of a nonadiabatic electronic transition to the ground state mediated by the solvent. The relative importance of these photofragment channels strongly depends on the cluster ion size. An  $\text{ICl}^-$  caged product is first observed for  $\text{ICl}^-(\text{CO}_2)_2$ , increasing rapidly to a maximum at  $n \approx 6$  and then decreasing. This caging efficiency is dramatically different from the  $\text{I}_2^-(\text{CO}_2)_n$  cluster ions where complete caging was observed for 16 solvent molecules. The  $\text{Cl}^-$  photofragment channel increases smoothly for the cluster size range studied and becomes the dominant channel for  $n=8$ . The relative yields of the  $\text{ICl}^-$  and  $\text{Cl}^-$  based products reflect the extent to which solvation influences the photodissociation pathways of  $\text{ICl}^-$ . © 1996 American Institute of Physics. [S0021-9606(96)00526-0]

## I. INTRODUCTION

The chemical properties of the solvent assert a profound influence on chemical reactions, especially those involving charge transfer and the ensuing solvent rearrangement about the newly formed ion. The role of solvation can be studied on a single molecule basis by examining solvent-mediated reactions in molecular clusters in the gas phase. This approach allows study of the stepwise effects of increasing solvation on the electronic structure of the chromophore<sup>1-6</sup> and intracuster reactivity.<sup>7-13</sup> Recent investigations of proton transfer reactions show that just a few solvent molecules can dramatically affect the outcome of a chemical reaction.<sup>7,8,11,12</sup> These studies showed that only three to four solvent molecules were required to induce proton transfer from the chromophore to the solvent.

Our approach involves the preparation of an ionic chromophore clustered with a specific number of solvent molecules, followed by photodissociation<sup>14-17</sup> of the chromophore. In order to determine how many solvent molecules are necessary to effect recombination of the dissociating core and the excitation energy dependence on the propensity of a given cluster to cage the dissociating diatom,<sup>18</sup> it is essential to synthesize and isolate clusters of specific composition. Ionic clusters are ideally suited for these experiments because size selection of the clusters can be achieved easily using standard mass spectrometric techniques. Many research groups have studied the solvation effects in cluster ion systems using this approach.<sup>19-27</sup> For example, Arnold *et al.*<sup>22</sup> have used photoelectron spectroscopy to examine

charge distribution changes in  $\text{I}^-(\text{CO}_2)_{n \leq 13}$  as the degree of ion solvation increases. Selegue and co-workers<sup>24</sup> measured the vibrational spectra of mass selected  $\text{Cs}^+[(\text{CH}_3)_2\text{CO}]_n(\text{CH}_3\text{OH})_m$  clusters and constructed a hydrogen bonding model between the acetone and methanol molecules surrounding the ionic core. Campagnola *et al.*<sup>26</sup> and Donnelly and Farrar<sup>27</sup> observed shifts in the absorption spectra of  $(\text{H}_2\text{O})_n^-$  and  $\text{Sr}^+(\text{NH}_3)_n$ , respectively, that are dependent on cluster size. These shifts are due to differential stabilization of the ground or excited states. Our work has focused on  $\text{ICl}^-$  photodissociation and cage recombination dynamics in size-selected  $\text{ICl}^-(\text{CO}_2)_n$  clusters.

In this article, we report the results of our ongoing studies of the solvation effects on the photodissociation of  $\text{ICl}^-$ . A primary motivation for these studies is to investigate the effects of the solvent on the charge distribution in a heteronuclear chromophore and compare it with a homonuclear ionic chromophore solvated by the same number of solvent molecules. Papanikolas *et al.*<sup>15,16</sup> have studied  $\text{I}_2^-(\text{CO}_2)_n$  cluster ions where the ionic core is totally symmetric and the charge is shared equally between the two iodine atoms. Their experiments and theoretical calculations showed that the first solvent molecules pack around the center of mass of the ionic core. As more solvent molecules are added, they tend to localize toward one end of the diatomic ion, polarizing the ionic charge distribution. This symmetric chromophore offers no control in the charge localization process. For  $\text{ICl}^-$ , the ionic core is no longer symmetric. The smaller Cl atom is solvated more efficiently, and therefore the first solvent molecules cluster about the Cl end of the diatom. This preferential solvation of the Cl atom will enhance the slight asymmetry in the initial charge distribution in the bare ion.

The photoabsorption cross section for  $\text{ICl}^-(\text{CO}_2)_4$  is

<sup>a)</sup>JILA Visiting Fellow, 1993-1994. Permanent address: Department of Physics and Astronomy, University of Iowa, Iowa City, IA 52242.

<sup>b)</sup>Electronic mail: wcl@jila.colorado.edu

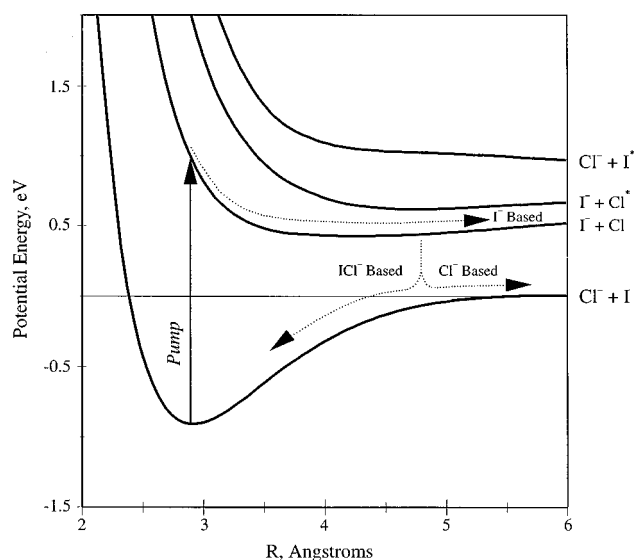


FIG. 1. Potential energy curves for  $\text{ICl}^-$  as determined by Parson and co-workers (Ref. 29). Only the  $1/2$  states (Hund's case (c)) are shown. The solid arrow labeled *Pump* indicates the transition used to photodissociate  $\text{ICl}^-$ . The dashed lines indicate the different photofragmentation pathways.

measured and compared with the bare  $\text{ICl}^-$  chromophore in order to investigate solvation effects on the electronic structure of the ionic core at internuclear distances close to the equilibrium distance. Comparison of the spectra suggests that the electronic structure of  $\text{ICl}^-$  is not significantly perturbed by the solvent at internuclear distances close to the equilibrium distance. The solvent does, however, perturb the electronic structure at larger I–Cl distances, as seen in the photofragmentation studies discussed below.

Detailed photofragmentation studies of  $\text{ICl}^-(\text{CO}_2)_n$ ,  $n=0-8$ , have been carried out at two wavelengths (644 nm and 740 nm). These wavelengths were chosen after measuring the photodestruction spectrum for bare  $\text{ICl}^-$ .<sup>28</sup> At these wavelengths,  $\text{ICl}^-$  is excited to a repulsive surface,<sup>29</sup> leading adiabatically to  $\text{I}^-$  and  $\text{Cl}$ , as shown in Fig. 1. Our results show that this continues to be the dominant reaction channel for  $\text{ICl}^-$  solvated by one or two  $\text{CO}_2$  solvent molecules. A larger number of  $\text{CO}_2$  solvent molecules dramatically affects the photofragmentation spectra, resulting in two new product channels. In addition to the  $\text{I}^-$  based direct photofragment, a solvent-induced recombination is observed to form  $\text{ICl}^-$ , and a solvated  $\text{Cl}^-$  product is also detected. These two new product channels are most likely the result of a nonadiabatic transition to the ground electronic state. This electron transfer process becomes more pronounced as the number of solvent molecules is increased, showing that it is a direct result of the strong coupling between the electronic and nuclear degrees of freedom. The relative yields of the  $\text{ICl}^-$  and  $\text{Cl}^-$  based products reflect the extent to which solvation influences the photodissociation pathways of  $\text{ICl}^-$ .

An important aspect of the present studies concerns the electron transfer induced by the surrounding solvent molecules from the iodine atom to the chlorine atom after photon absorption. Electron transfer occurs as an electron localized

on a donor site transfers to a state localized on an acceptor site. The first theories describing the role of the solvent on the kinetics of electron transfer processes, derived by Marcus,<sup>30</sup> were classical in nature and within the framework of dielectric continuum theory. Newton and Sutin<sup>31</sup> provided an excellent review of the foundations of electron transfer theories. Also, extensive theoretical work has been done on problems in which the coupling of the solute electronic structure to the solvent environment plays an important role in determining the outcome of the reaction. Sheu and Rossky<sup>32</sup> have developed a method to simulate the charge-transfer-to-solvent spectrum of aqueous  $\text{I}^-$ . Keirstead and co-workers<sup>33</sup> have studied the  $S_N1$  ionization reaction ( $\text{RX} \rightarrow \text{R}^+ + \text{X}^-$ ) in solution. As this reaction proceeds, the electronic wave function evolves from a covalent form to an ionic form. This latter form is coupled to the solvent through long-range electrostatic interaction.

We report the observation of electron transfer within an anionic chromophore mediated by the surrounding solvent molecules. In this system, there is very little charge delocalization onto the solvent. In contrast, charge delocalization onto the solvent is often observed in homogenous clusters, for example, in cluster ions such as  $(\text{O}_2)_n^-$ , for which photoabsorption of the larger cluster results from charge transfer between the  $\text{O}_4^-$  ionic core and the  $\text{O}_2$  solvent ligand.<sup>34</sup> Chens and coworkers<sup>35</sup> have studied the heterogenous molecular clusters of benzene(s)–iodine and other complexes, and have observed charge transfer from the benzene onto the  $\text{I}_2$ . Moreover, photon-assisted charge transfer reactions are often observed in cationic clusters.<sup>36-38</sup> Shen and Farrar<sup>38</sup> have studied the size-dependent effects in the photodissociation spectra of  $\text{Sr}^+(\text{NH}_3)_n$  and have proposed an intramolecular electron transfer mechanism to account for the observed spectral features. These charge transfer to solvent (or vice versa) transitions are also common in solution.<sup>39-41</sup>

In Sec. II of this article, we provide a brief description of the cluster ion machine and tandem time-of-flight mass spectrometer used for this work. A brief review of previous experiments with  $\text{ICl}^-$  is given in Sec. III. In Sec. IV, the results of new studies of the photoabsorption and photofragmentation of  $\text{ICl}^-(\text{CO}_2)_n$  cluster ions are presented. Finally, in Sec. V we summarize the major findings and present prospects for future studies.

## II. EXPERIMENT

### A. Overview

A schematic diagram of the cluster ion source and tandem time-of-flight (TOF) mass spectrometer is shown in Fig. 2. The  $\text{ICl}^-(\text{CO}_2)_n$  cluster ions are created by crossing a pulsed free jet expansion with a continuous  $\sim 1$  keV electron beam. The initially formed ions drift for  $\sim 15$  cm in the cold expansion while growing a solvent shell. At this point, a pulsed electric field injects the ions into a Wiley–McLaren TOF mass spectrometer. At the spatial focus of the primary TOF, the 3000 eV ions intersect a pulsed laser beam. The resulting ionic photofragments are analyzed in a single-field reflectron TOF mass analyzer (the secondary TOF) and de-

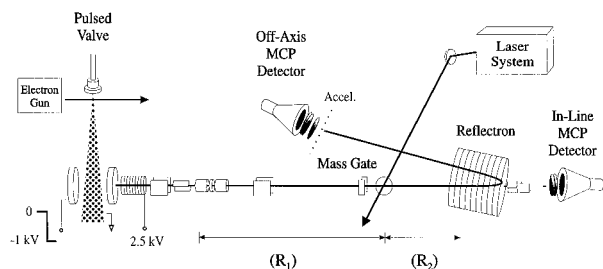


FIG. 2. Schematic representation of the cluster ion source and tandem time-of-flight mass spectrometer.

tected at an off-axis detector. Either the precursor ions or neutral photofragments are detected at the in-line detector. Details of the experiment and the data collection procedures are given below.

### B. Cluster ion source and primary TOF mass analysis

$\text{ICl}^-(\text{CO}_2)_n$  cluster ions are formed by passing neat  $\text{CO}_2$  at pressures of 1–2 atm through a reservoir containing  $\text{ICl}$ . The reservoir consists of a stainless steel (SS) bubbler containing a glass tube in which the  $\text{ICl}$  was deposited. While the bubbler was left at ambient temperature, the SS lines inside the chamber were mildly heated to a few degrees above room temperature to avoid clogging (the melting point of  $\text{ICl}$  is 27 °C). The  $\text{ICl}/\text{CO}_2$  gas mixture is expanded supersonically through a pulsed valve (General Valve, Series 9) with a nozzle diameter of 800  $\mu\text{m}$ . The temperature of the pulsed valve body was kept a few degrees higher than the connecting SS lines to avoid condensation inside the valve. The inner parts of the pulsed valve were carefully chosen because  $\text{ICl}$  is a corrosive, moisture-sensitive compound. The armatures were gold plated and poppets were made of Teflon. The pulsed free jet expansion is crossed with a continuous 400  $\mu\text{A}$  beam of  $\sim 1$  keV electrons about 7 mm in diameter. The ions of interest are formed by attachment of secondary electrons to  $\text{ICl}$ . Larger cluster ions grow via  $\text{CO}_2$  condensation around the  $\text{ICl}^-$  ionic core.<sup>42</sup> The temperature of these cluster ions is estimated to be  $\sim 50$  K using RRKM calculations.<sup>43</sup>

After the ions drift for around 15 cm ( $\sim 1$  ms) in the expansion, at which point a transverse pulsed electric field ( $-1$  keV) injects the negative ions into a differentially pumped Wiley–McLaren TOF mass spectrometer. The second stage of the TOF consists of an acceleration lens stack where the ions receive an additional 2500 eV of kinetic energy. The ions thus acquire a kinetic energy of  $(3000 \pm 200)$  eV. After this stage, the ions enter the field-free region ( $R_1$ ) where the ions are separated according to their masses. In this region, the ions pass through a set of horizontal deflectors to compensate for most of the axial kinetic energy imparted by the supersonic expansion. The ions then pass through a set of vertical deflectors for steering, followed by an einzel lens biased in a mild decelerating mode to provide a transverse focus at the Wiley–McLaren longitudinal focus of the primary TOF. A second set of horizontal deflectors

affects a  $1.5^\circ$  bend in the ion beam, which separates the fast ions from the neutral particles and reduces the background noise at the in-line detector. The ion beam is crossed with a pulsed laser beam at the spatial focus of the mass spectrometer, which occurs at  $\sim 1.5$  m from the entrance of the second stage of the TOF and  $\sim 16$  cm before the reflectron entrance ( $R_2$ ).

### C. Photolysis, secondary mass analysis, and detection

The ionic clusters arrive at the spatial focus of the primary TOF at a time determined by their mass. Therefore, adjustment of the time delay between the extraction and nanosecond laser pulses provides unambiguous mass-selected photoexcitation. The mass gate, two parallel plates with one biased at the beam potential and the other one pulsed to 2300 V, is located just in front of the laser interaction region. Its purpose is to reject unwanted precursor ions, thus reducing the background noise.

Nanosecond laser pulses are generated by using the 30 Hz frequency-doubled output (250 mJ/pulse) of a Quanta Ray GCR3 Q-switched Nd:YAG laser to pump a homemade dye laser. The dye oscillator was constructed from a Lambda Physik dye laser, complete with holographic grating, magnifying telescope, and output coupler. Approximately 10% of the Nd:YAG energy is used to pump the dye laser oscillator. The remainder of the dye laser consists of two amplification stages. The first stage is side pumped, receiving 20% of the initial pump laser beam energy. The second stage is end pumped with 70% of the pump energy in order to improve the laser beam spatial profile. A telescope is used to collimate the output laser beam. The output of the dye laser is typically 5–8 mJ/pulse in the near-infrared spectral range of these studies. Exciton dyes (DCM, LDS 698, 720, 740) are used as gain media. The amplified spontaneous emission (ASE) is reduced by placing spatial filters after each amplification stage, reducing the ASE to  $< 2\%$  of the total pulse energy.

After photolysis, mass analysis of the ionic photofragments is achieved with the secondary TOF reflectron mass spectrometer.<sup>44</sup> Ionic photofragments are detected at the off-axis microchannel plate detector. Five grids are located in front of the detector. A small potential,  $\sim 200$  V, is applied to the first grid plate to discriminate against low-energy electrons. The remaining grids form a post-acceleration stack that gives the ions an additional 1000 eV of kinetic energy, improving the detector efficiency. The detector gain is  $\sim 10^6$ .

The neutral detector (in-line detector) consists of microchannel plates and is located behind both the reflectron and a set of vertical and horizontal deflectors. Both the in-line and off-axis detectors are biased at high voltage, therefore the ion signal is capacitively coupled to the pulse-processing electronics. The ion signal is pre-amplified by a factor of 10, then amplified by a variable amplifier and finally sent to a transient digitizer or analog to digital converter controlled by a computer.

Figure 3 shows a parent ion mass spectrum taken under

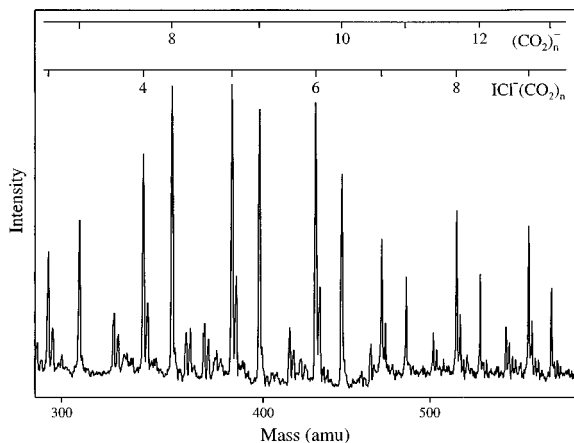


FIG. 3. Negative ion mass spectrum observed with a  $\text{ICl}/\text{CO}_2$  gas mixture. The major species are  $(\text{CO}_2)_n^-$  and  $\text{ICl}^-(\text{CO}_2)_n$  cluster ions.

typical conditions as described previously. The mass spectrum was acquired with a transient digitizer/signal averager. The mass resolution,  $m/\Delta m$ , is around 800. Two classes of cluster ions dominate the mass spectrum:  $\text{ICl}^-(\text{CO}_2)_n$  and  $(\text{CO}_2)_n^-$ . In addition,  $\text{Cl}_3^-(\text{CO}_2)_n$  cluster ions are present in the lower mass region, while  $\text{Cl}^-(\text{CO}_2)_n$  cluster ions are present in the higher mass region. Multiplets due to the isotopes of chlorine in the ratio of  $^{35}\text{Cl}:^{37}\text{Cl} \sim 3:1$  are easily resolved up to mass 800, making the assignment of this portion of the mass spectrum especially easy. Although only a segment of the mass spectrum is shown,  $\text{ICl}^-(\text{CO}_2)_n$  cluster ions up to  $n=15$  are readily produced.

#### D. Data collection procedures

Two basic types of data are presented in this article: photodissociation cross section measurements and ionic photofragmentation yields from the cluster ions. The data acquisition methods for these data types are briefly discussed.

Relative photodestruction cross sections for  $\text{ICl}^-(\text{CO}_2)_4$  were obtained by monitoring the appearance of neutrals at the in-line detector. This neutral signal was normalized to the  $\text{ICl}^-(\text{CO}_2)_4$  ion current measured at the off-axis detector and the laser intensity. Four different dyes were necessary to measure the photodissociation spectrum, and measurements made with a given dye were scaled to the others based on cross sections determined in overlapping regions. An absolute photodissociation cross section was determined at 644 nm via photodepletion<sup>45,46</sup> of the precursor ion signal monitored at the off-axis detector, e.g., [precursor ion(*laser off*)–precursor ion(*laser on*)] and the laser fluence was monitored with a photodiode. Power dependence studies were carried out to avoid saturation limits and multiphoton processes. The entire spectrum was then scaled. Cross sections were extracted based on the Beer–Lambert law. All of the photodissociation cross section measurements were obtained in a sequence with the laser pulses on and off to provide background subtraction. The statistical fluctuations in the relative measurements and in the absolute cross sections are

about 15%. The absolute cross sections are sensitive to systematic effects such as the laser-ion beam overlap and the homogeneity of the laser beam. The absolute cross section measurement uncertainties are approximately a factor of 2.

The photofragmentation data were collected as follows. A specific precursor ion, for example,  $\text{ICl}^-(\text{CO}_2)_8$ , was selected by using the pulsed mass gate. The laser timing was adjusted to allow the laser pulses to irradiate the precursor cluster ion of interest. The reflectron voltage was adjusted to refocus the photofragment ion of interest and the laser timing was optimized by observing the production of a given photofragment on an oscilloscope. By adjusting the electrostatic potential on the reflectron, the fragment ion of interest spent the same time in transit to the off-axis detector as the precursor ion, providing an unambiguous fragment ion mass determination. Careful photofragmentation studies were carried out for each of the two Cl isotopes. No differences were observed. The results presented below are for the dominant  $^{35}\text{Cl}$  isotope. For data acquisition, we first determined all the possible photofragment ions for a given precursor ion. We then took  $n$  data cycles, where  $n$  represents the number of different photofragments from a precursor ion. The first fragment of the different data cycles was varied to correct for any drift in the precursor ion current. The yield of each ionic fragment in each cycle was averaged for 800 laser shots and then the spectrum was integrated. Typical statistical errors in the fragment yield are about 3%. Power dependence studies were carried out to avoid saturation limits and multiphoton processes.

### III. PREVIOUS STUDIES OF $\text{ICl}^-$

Preliminary work has been carried out on the bare  $\text{ICl}^-$  ion to characterize the chromophore.<sup>47</sup> In this section, a brief summary of these results is provided. Potential energy curves<sup>29</sup> for  $\text{ICl}^-$ , obtained using all-electron multireference configuration interaction (MRCI) calculations, are shown in Fig. 1. The ion has a formal bond order of  $\frac{1}{2}$ , and a total angular momentum,  $\Omega$ , of  $\frac{1}{2}$  for the ground state. The equilibrium bond length and vibrational frequency are calculated to be  $\sim 2.91$  Å and  $\sim 185$   $\text{cm}^{-1}$ , respectively. All of the low-lying excited states are either dissociative or have extremely shallow wells. Photodissociation of  $\text{ICl}^-$  is more complex than that of  $\text{I}_2^-$  because of the broken symmetry, which provides twice as many distinct exit channels. There are four low-lying dissociative excited states: two asymptotes correspond to the production of  $\text{I}^-$ . These surfaces are separated by the spin-orbit coupling<sup>48</sup> of the Cl atom, 0.11 eV. The other two states correspond to the formation of  $\text{Cl}^-$  and  $\text{I}$  or  $\text{I}^*$ , and are split<sup>48</sup> by 0.94 eV.

The potential energy curves provide qualitative information concerning the electronic structure of solvated  $\text{ICl}^-$  near the equilibrium I–Cl distance. In the presence of solvent, caution must be exercised if these curves are extrapolated to large internuclear separation, where the important dynamics occur. The arrow labeled *Pump* in Fig. 1 shows the expected  ${}^2\Pi_{1/2} \leftarrow {}^2\Sigma_{1/2}^+$  transition for absorption in the red (600–700 nm) spectral region. The visible absorption spectrum of  $\text{ICl}^-$ ,

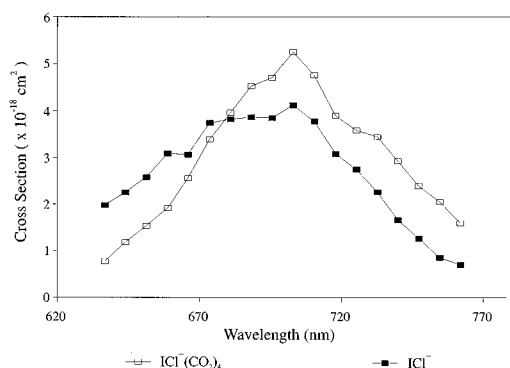


FIG. 4. Absolute  $\text{ICl}^-$  and  $\text{ICl}^-(\text{CO}_2)_4$  photodestruction cross sections for the transition labeled *Pump* in Fig. 1. The statistical fluctuations in the relative and absolute cross sections are about 15%. The absolute measurements uncertainties are approximately a factor of two.

shown in Fig. 4, is a featureless broadband with a FWHM of 90 nm, peaking around 700 nm with a peak cross section of  $(3.9 \pm 0.3) \times 10^{-18} \text{ cm}^2$ . Throughout this band,<sup>47</sup> photodissociation of bare  $\text{ICl}^-$  produces only  $\text{I}^-$  ionic products, although at the red end of the spectrum, starting at around 740 nm, the products include 3% Cl due to a weak transition to the lowest  $\frac{3}{2}$  excited state. It is possible that either a solvent-induced shift in the curves or an enhancement in this transition strength due to the electric field of the solvent could make this process more important in the clusters.

The bond strengths of  $\text{ICl}^-$  and  $\text{I}_2^-$  are  $(1.07 \pm 0.02) \text{ eV}$  and  $(1.24 \pm 0.04) \text{ eV}$ , respectively, as determined by analyzing the neutral fragment recoil velocity following photodissociation.<sup>47</sup> The adiabatic electron affinity of ICl is  $(2.53 \pm 0.03) \text{ eV}$  as determined from the bond strengths of  $\text{ICl}^-$  and ICl, and the electron affinity of Cl. The electron affinity of  $\text{I}_2$  has been determined to be  $(2.69 \pm 0.05) \text{ eV}$  from a charge transfer energy threshold experiment.<sup>49</sup> Both properties are thus comparable for  $\text{ICl}^-$  and  $\text{I}_2^-$ . Furthermore, the charge distributions on the bare ions are similar: for  $\text{I}_2^-$ , the Mulliken charge is 0.50 on each atom, whereas for  $\text{ICl}^-$ , the Mulliken charge is 0.55 on the Cl atom and 0.45 on the I atom.<sup>29</sup> The major difference between the  $\text{I}_2^-$  and  $\text{ICl}^-$  cores is in the atomic radii. The ionic radius<sup>50</sup> for  $\text{I}^-$  is 2.20 Å and that for  $\text{Cl}^-$  is 1.81 Å. The 0.39 Å difference in size for the case of  $\text{ICl}^-$  plays an important role in determining the  $\text{ICl}^-(\text{CO}_2)_n$  cluster ion structure.

#### IV. RESULTS AND DISCUSSION

The experiments described here investigate the effect of the solvent on the charge distribution in the ionic chromophore,  $\text{ICl}^-$ , and the concomitant effect on the photodissociation dynamics. In Sec. IV A, we report the photodestruction spectrum of  $\text{ICl}^-(\text{CO}_2)_4$ . The role of the solvent in the photodissociation of  $\text{ICl}^-(\text{CO}_2)_n$  cluster ions is discussed in Sec. IV B.

#### A. Photoabsorption spectrum and electronic structure of $\text{ICl}^-(\text{CO}_2)_4$

The absorption spectrum of  $\text{ICl}^-(\text{CO}_2)_4$  was measured in order to study the effect of solvation on the electronic structure of the ionic chromophore at internuclear distances close to equilibrium distance,  $r_e$ . Solvent effects may be observed if the absorption spectrum of the cluster ion shifts with respect to that of the bare ion. The  $\text{ICl}^-(\text{CO}_2)_4$  case was chosen for two reasons. First, the direct  $\text{I}^-$  photofragments are not observed with this cluster ion. Second, Monte Carlo structural calculations suggest that the maximum asymmetric solvation of the Cl end occurs for about 4–6 solvent molecules.<sup>29</sup> Such structures will have the greater solvent electric field perturbation on the  $\text{ICl}^-$  electronic states.

The photoabsorption cross sections of  $\text{ICl}^-(\text{CO}_2)_4$  and  $\text{ICl}^-$  for the spectral range 630 to 770 nm, corresponding to the pump transition in Fig. 1, are shown in Fig. 4. The  $\text{ICl}^-(\text{CO}_2)_4$  spectrum extends from  $\sim 620$  to  $\sim 780$  nm, peaking at around 700 nm with an absorption cross section of  $(5.3 \pm 2.1) \times 10^{-18} \text{ cm}^2$ . From these studies, we conclude that the visible absorption spectra of  $\text{ICl}^-(\text{CO}_2)_4$  and  $\text{ICl}^-$  are very similar with a  $\sim 10$  nm red shift, implying that the solvent does not significantly distort the  $\text{ICl}^-$  potentials near  $r = r_e$ . The long wavelength edges of both spectra overlap almost exactly, but the clustered  $\text{ICl}^-$  cross sections decrease faster along the blue edge. Because the  $\text{ICl}^-(\text{CO}_2)_4$  absorption spectrum is not broader, it does not seem likely that other excited states are involved, but rather that only the ground and one excited state are slightly distorted. The difference in the relative intensity of the two bands is within the error limits. Therefore, either the asymmetric  $\text{CO}_2$  solvation does not strongly perturb the electronic structure of the ionic core at internuclear distances close to  $r_e$ , or the solvent perturbs both the ground and excited states equally. In either case, it is likely we are accessing the same excited state.

This result suggests that  $\text{ICl}^-$  remains the ionic chromophore in the cluster and that there is little charge delocalization from  $\text{ICl}^-$  onto the  $\text{CO}_2$  solvent. This is not surprising since  $\text{CO}_2^-$  is unstable<sup>51</sup> by 0.6 eV with respect to  $\text{CO}_2 + e^-$ . For larger clusters, charge delocalization onto the solvent may occur. DeLuca and co-workers<sup>52</sup> have measured photoelectron spectra of  $(\text{CO}_2)_n^-$  clusters,  $n=2-13$ , and observed that the electron affinity of the corresponding neutral cluster is less than  $\approx 2.2 \text{ eV}$ . Recent photoelectron spectra of  $\text{I}^-(\text{CO}_2)$  show a weak excitation of the  $\text{CO}_2$  bending motion,<sup>22</sup> implying a minimal charge delocalization from  $\text{I}^-$  onto the solvent. Additional measurements on larger clusters are required before the effect of the solvent on the electronic structure of  $\text{ICl}^-$  can be fully understood.

#### B. $\text{ICl}^-(\text{CO}_2)_n$ photofragmentation studies at 644 and 740 nm

Nanosecond photofragmentation experiments of  $\text{ICl}^-(\text{CO}_2)_n$  cluster ions ( $n=0-8$ ) have been carried out to probe the “static” aspects of the photoinduced dissociation. In these experiments, the transition labeled as *Pump* in Fig. 1 is excited. The excitation energies employed are well above

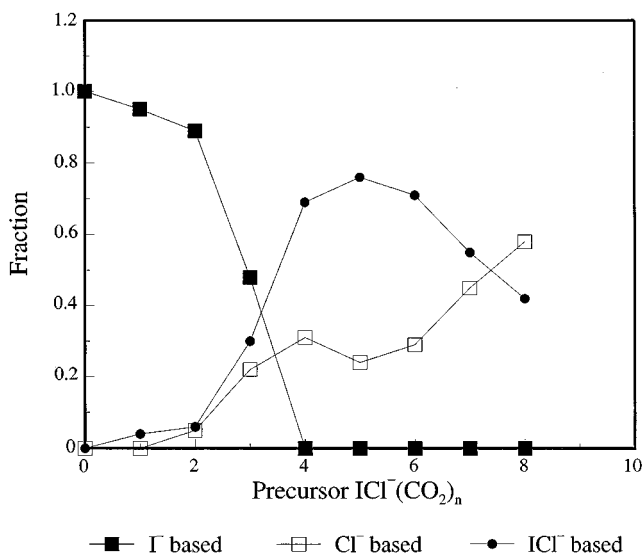
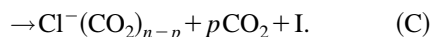
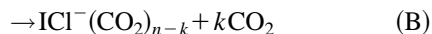
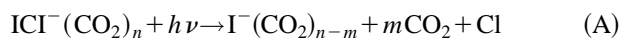


FIG. 5. Photofragmentation products for  $\text{ICl}^-(\text{CO}_2)_n$  cluster ions at 644 nm.

the  $\text{ICl}^-$  dissociation limit. For example, using 644 nm excitation, there is a 0.8 eV of total kinetic energy release on the excited state surface. From conservation of linear momentum, as the diatomic ion dissociates, the Cl atom acquires  $\sim 75\%$  of the total kinetic energy release.

We have observed three different photodissociation channels:



Each of the channels typically spans a range of about two or three solvent molecules and depends strongly on the excitation energy. For example, channel (B) for  $\text{ICl}^-(\text{CO}_2)_5$  at 644 nm produces  $\text{ICl}^-$  and  $\text{ICl}^-(\text{CO}_2)$  in a ratio of approximately 2:1, but does not produce other cluster sizes. Channel (A) corresponds to the expected  $\text{I}^-$  based photoproducts, and this is the dominant channel for the smaller  $\text{ICl}^-(\text{CO}_2)_{n \leq 2}$  cluster ions. This direct photofragmentation pathway was also observed in the  $\text{I}_2^-(\text{CO}_2)_{n \leq 15}$  cluster ion experiments,<sup>15</sup> and the products were named “uncaged” products.

Channels (B) and (C) correspond to the solvent induced nonadiabatic transition to the ground electronic state, leading to an asymptote of  $\text{Cl}^- + \text{I}$ , as shown in Fig. 1. Therefore, after excitation to an  $\text{I}^-$  correlated state, the charge has to transfer from the I to the Cl atom. Channel (B) corresponds to solvent-induced recombination of the dissociating  $\text{ICl}^-$  molecule, which is the dominant channel for the cluster sizes  $4 \leq n \leq 7$ . This channel leads to ions called the “caged product” in the  $\text{I}_2^-$  studies. The possibility of charge transfer and subsequent dissociation of the complex is demonstrated by the appearance of solvated  $\text{Cl}^-$  products, channel (C). This type of product might also occur for the symmetric  $\text{I}_2^-$  based clusters, but it would not have been observable due to the indistinguishability of the two iodine atoms. Channel (C)

TABLE I. Summary of the most prominent photofragment ion from  $\text{ICl}^-(\text{CO}_2)_n$  cluster ions after absorption of a 644 nm photon.

$\text{ICl}^-(\text{CO}_2)_n$	$\text{I}^-(\text{CO}_2)_n^a$	$\text{Cl}^-(\text{CO}_2)_n^a$	$\text{ICl}^-(\text{CO}_2)_n^a$
2	1	2	0
4	none	3	0
6	none	5	1
8	none	7	2

<sup>a</sup>The numbers represent the most prominent photofragment ion. This fragment ion is typically near the center of the photofragment ion distribution, which is two or three  $\text{CO}_2$  monomers wide.

first appears at  $n \geq 2$  and becomes dominant as the number of  $\text{CO}_2$  solvent molecules is increased. The fraction of ions that dissociate by channel (B) or (C) indicates the extent to which the solvent molecules are able to “follow” the charge as it migrates from one end of the chromophore to the other, as discussed below. Both channels arise solely from the influence of the solvent on the  $\text{ICl}^-$  photodissociation pathways. They are strongly coupled to each other due to their dependence on the interaction of the ionic core with the solvent and they compete with each other. The fractional yields of the different product channels (obtained by summing all of the products) from the photofragmentation studies at 644 nm excitation energy are summarized in Fig. 5. Table I lists the major ionic photofragments produced after absorption of a 644 nm photon for precursor ions having up to eight  $\text{CO}_2$  molecules.

### 1. Charge transfer induced by the solvent

A nonadiabatic electronic transition to the ground state must occur in order to produce either  $\text{Cl}^-$  or  $\text{ICl}^-$  based products after excitation to the repulsive state leading to  $\text{I}^- + \text{Cl}$ . A plausible mechanism is given below and is shown schematically in Fig. 6. The initial structure of  $\text{ICl}^-(\text{CO}_2)_4$ , has all of the solvent molecules clustered around the smaller

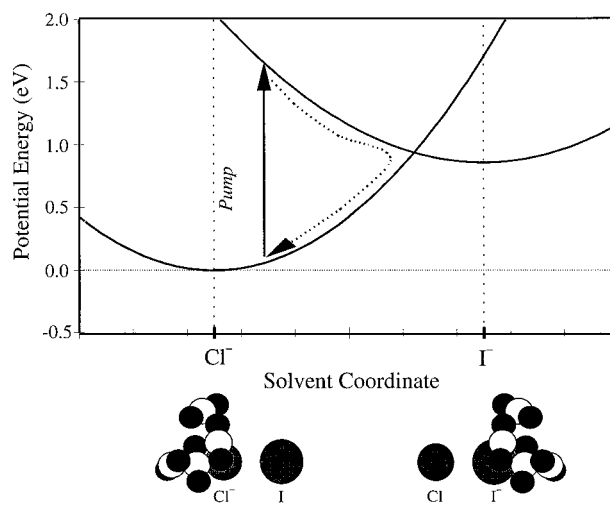


FIG. 6. Schematic representation of the potential energy for  $\text{ICl}^-(\text{CO}_2)_4$  as a function of the solvent coordinate, specifically for the cases where the charge is localized on the Cl end and on the I end. The dotted line is intended to show the nonadiabatic transition to the ground state.

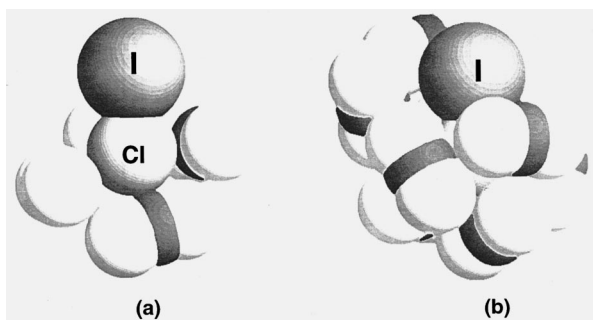


FIG. 7. Lowest energy structures observed for (a)  $\text{ICl}^-(\text{CO}_2)_4$  and (b)  $\text{ICl}^-(\text{CO}_2)_8$ .

Cl end, as shown in Fig. 7(a), inducing some additional localization of the charge on the Cl atom. The charge, which was initially slightly larger on the Cl, transfers to the iodine following absorption of a red photon. In the limit for which the dissociating diatom remains at close internuclear distances, the solvent has time to adjust to the new configuration before dissociation by moving toward the newly formed ion. The interaction between the  $\text{ICl}^-$  and the  $\text{CO}_2$  molecules is a strong, long-range attraction, varying as  $1/r^3$ . Because the larger  $\text{I}^-$  ion will be stabilized less by solvation than the  $\text{Cl}^-$ , and the electron binding energy is less for  $\text{I}^-$ , there will be a time late in the solvent reorganization process when it is thermoneutral for the electron to transfer back to the Cl atom. This curve crossing occurs along the solvent coordinate at a solvent configuration that preferentially stabilizes the I end and not the Cl end. The rate-limiting step for the electron to transfer back to the Cl atom is likely the rate at which the solvent molecules are capable of following the charge and solvating the newly-formed ion. This mechanism would lead to  $\text{ICl}^-$  or  $\text{Cl}^-$  based products at a wavelength where the direct photoproduct was  $\text{I}^-$ . These new charge transfer channels turn on at  $n \approx 2$ , as shown in Fig. 5. Depending on the I–Cl distance at this time, there may be a significant probability for this curve crossing to occur. The experimental data show that this crossing probability is 100% for  $\text{ICl}^-(\text{CO}_2)_4$  at an excitation energy of 1.93 eV. Another plausible mechanism for the production of  $\text{Cl}^-$  based products will be the coupling of the  $\text{I}^- + \text{Cl}$  with the upper dissociative  $\text{Cl}^- + \text{I}^*$  state at large internuclear distance. This mechanism will be explored in a forthcoming paper.

The driving force for the nonadiabatic electronic transition to the ground state primarily derives from the differential solvation energy of  $\text{Cl}^-$  and  $\text{I}^-$  at large internuclear separations. The Born equation<sup>53</sup> identifies the electrical work required to transfer an ion from vacuum into a liquid medium treated as a continuum dielectric medium. That is:

$$\Delta G_{\text{solv}} = \frac{(ze)^2}{(8\pi\epsilon_0)r} \left( 1 - \frac{1}{\epsilon} \right), \quad (1)$$

where  $\epsilon_0$  is the permittivity of vacuum,  $z$  is the number of elementary charges  $e$ ,  $r$  is the radius of the ion, and  $\epsilon$  is the relative permittivity of the bulk dielectric constant of the liquid medium. This equation indicates that a smaller ion

will have a larger solvation energy. Thus, the difference between the solvation energy of  $\text{Cl}^-$  and  $\text{I}^-$  is largely due to the 0.39 Å differences in ionic radii. The absolute standard molar Gibbs free energy at 298.15 K for  $\text{I}^-$  is  $-283$  kJ/mol and for  $\text{Cl}^-$  is  $-347$  kJ/mol in the bulk limit.<sup>53</sup>

Marcus<sup>30</sup> showed that the rate of electron transfer is dependent on the distance between donor and acceptor, the reaction exothermicity, the solvent reorganization energy, and the time scale for relaxation of the solvent coordinate. In the limit of  $KT \gg h\nu_{\text{vib.}}$ , the Marcus equation for the electron transfer rates,  $K_{\text{ET}}$ , is

$$K_{\text{ET}} = \frac{1}{\tau_s} \exp\left(-\frac{(\lambda + \Delta G^0)^2}{4\lambda RT}\right), \quad (2)$$

where  $\tau_s$  is the time scale for relaxation of the solvent coordinate,  $\Delta G^0$  is the reaction free energy, and  $\lambda$  is the solvent reorganization energy defined as

$$\lambda = \frac{(\Delta e)^2}{2} \left( \frac{1}{r_a} + \frac{1}{r_d} - \frac{2}{r} \right) \left( \frac{1}{n^2} - \frac{1}{\epsilon_s} \right). \quad (3)$$

In Eq. (3), the electron acceptor and donor of radii  $r_a$  and  $r_d$ , respectively, are separated by a distance  $r$ ,  $\Delta e$  is the magnitude of the charge being transferred, and  $n^2$  and  $\epsilon_s$  are the optical and static dielectric constants, respectively. The solvent reorganization energy results from the response of the solvent localized charge distributions (e.g., solvent dipoles) to the influence of the static electric field produced by the newly formed ion. The solvent dipoles will align to counter the ion's electric field, and this interaction will induce an internuclear distance-dependent shift in the energy levels of the ion. This shift in the energy levels of the ions may be sufficient to allow the electron to transfer from the donor to the acceptor site. Sometimes, the solvent can reorganize around the newly formed ion in such a way that the electron can transfer back to its original position.<sup>54,55</sup> In our case, solvent reorganization results in the electron transferring from the nascent  $\text{I}^-$  photoproduct back to the Cl atom in the ground state surface.

**$\text{ICl}^-$  vs  $\text{Cl}^-$  production.** The solvent reorganization is responsible for electron transfer from the  $\text{I}^-$  back to the Cl in the stretched diatom. In this process, the dissociating molecule can recombine, forming a solvated  $\text{ICl}^-$ , or can dissociate, forming a solvated  $\text{Cl}^-$ . The  $\text{ICl}^-$  branching fraction reflects the ability of the solvent molecules to effect recombination of the dissociating molecule. The branching ratio for production of  $\text{ICl}^-$  based fragment ions versus cluster size at two different wavelengths corresponding to 0.8 eV (644 nm) and 0.6 eV (740 nm) of total kinetic energy release on the excited state surface is plotted in Fig. 8. Two distinct behaviors are apparent in this plot. The fraction caged for small clusters,  $n \leq 4$ , decreases significantly with increasing excitation energy. At 644 nm, the caging efficiency for  $\text{ICl}^-(\text{CO}_2)_4$  is around 67%, whereas for 740 nm it is 88%. The caging fraction increases as the number of  $\text{CO}_2$  molecules is increased, reaching a maximum around four or five solvent molecules and then rapidly decreasing as the number of solvent molecules is increased. The decrease in the caging frac-

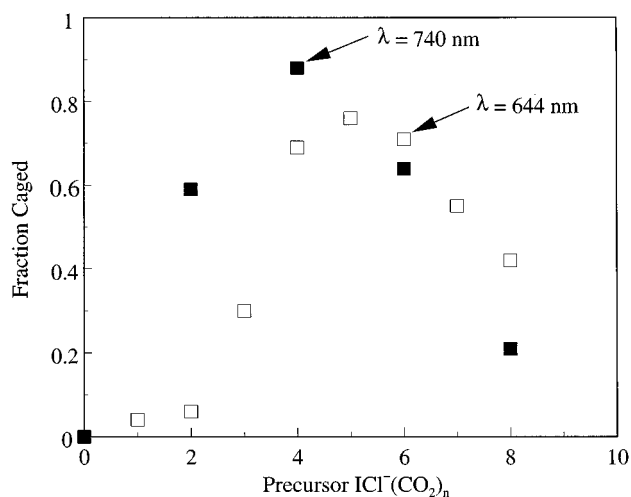


FIG. 8. The branching ratio for production of  $\text{ICl}^-$  based products as a function of precursor cluster ion size for 644 and 740 nm of excitation energy.

tion is concomitant with the increased production of solvated  $\text{Cl}^-$ . Also, the caging fraction for cluster ions with six or more solvent molecules is larger for higher excitation energy.

One might expect that as the number of solvent molecules is increased the caging efficiency would continue to increase. This behavior was observed for  $\text{I}_2^-(\text{CO}_2)_n$ , reaching complete caging for 16 solvent molecules. The decrease in the caging fraction as the number of solvent molecules increases was quite unexpected and different from what was observed<sup>15</sup> for  $\text{I}_2^-$ , as will be shown below. Because the bond strengths of  $\text{ICl}^-$  and  $\text{I}_2^-$  are comparable, any explanation must lie either in the size difference between Cl and I or in the better mass match between Cl and  $\text{CO}_2$ , as compared to I and  $\text{CO}_2$ . The better mass match allows more efficient energy transfer to a  $\text{CO}_2$  located on the Cl end of  $\text{ICl}^-$ , and the size difference makes  $\text{Cl}^-$  solvation energetically preferable to  $\text{I}^-$  solvation.

The ground state  $\text{ICl}^-(\text{CO}_2)_n$  potential energy surface has two significant minima separated by a barrier that represents the solvation difference between the two ions, one corresponding to solvated  $\text{ICl}^-$  and a second corresponding to solvated  $\text{Cl}^-$  and an iodine atom. While the global minimum on the surface is for solvated  $\text{ICl}^-$ , the dissociation process will very likely access the  $\text{Cl}^-$  minimum due to the excess kinetic energy. One might well expect that the absolute size of the barrier between these minima will be increasingly hard to surmount as the number of  $\text{CO}_2$  solvent molecules is increased. Qualitative simulations of the dissociation dynamics suggest a high probability that the photoexcited complex can be trapped in the  $\text{Cl}^-$  minimum, and that the concerted solvent motion and electron redelocalization required to reach the global minimum is unlikely on the time scale of the experiment ( $\sim 10$   $\mu\text{s}$ ). For cluster ions with more than six solvent molecules, the caging fraction is larger for higher excitation energy. As more energy is deposited into the cluster, it appears that the dissociating  $\text{ICl}^-$  has a better chance

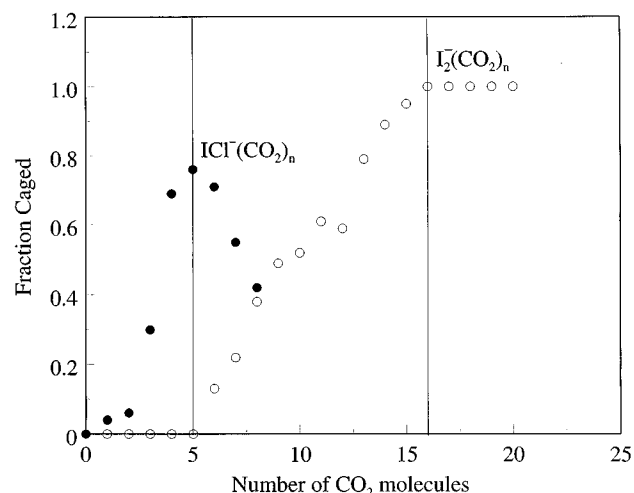


FIG. 9. Comparison of the  $\text{ICl}^-(\text{CO}_2)_n$  at 644 nm and  $\text{I}_2^-(\text{CO}_2)_n$  at 720 nm caging fractions. The photon energies were chosen so that the kinetic energy release of the iodine atom was similar (0.3 eV) for both ionic chromophores.

to surmount the ground state barrier and recombine.

The formation of a solvent-separated species<sup>56,57</sup> will also produce solvated  $\text{Cl}^-$ . After the charge has transferred to the Cl atom, the  $\text{CO}_2$  molecules packed around the middle of the  $\text{ICl}^-$  could move between the dissociating molecule, efficiently solvating the  $\text{Cl}^-$  end. This arrangement decreases the probability for the  $\text{ICl}^-$  to recombine.

## 2. $\text{I}_2^-$ vs $\text{ICl}^-$ recombination efficiency

Here we compare the recombination efficiency for  $\text{ICl}^-$  and  $\text{I}_2^-$  in the presence of  $\text{CO}_2$  solvent molecules. Measurement of the caging fraction as a function of cluster size provides a microscopic picture of the ability of the solvent molecules to induce recombination. Figure 9 depicts the caging fraction for  $\text{ICl}^-$  at 644 nm and  $\text{I}_2^-$  at 720 nm<sup>15</sup> as a function of the number of  $\text{CO}_2$  molecules. The photon energies were chosen so that the kinetic energy release on the excited state surface of the iodine atom was similar (0.3 eV) for both ionic chromophores. It is apparent in Fig. 9 that the caging for  $\text{ICl}^-$  increases rapidly, and that even one solvent molecule is capable of arresting the dissociating  $\text{ICl}^-$ . The caging fraction channel becomes increasingly important as the number of solvent molecules is increased, until it reaches a maximum of 70% at  $n=6$ . For  $n>6$ , the caging channel becomes less important. This behavior sharply contrasts with that of  $\text{I}_2^-$ , where the caged fraction is zero for  $n\leq 5$ . Moreover, while the caging fraction for  $\text{ICl}^-$  decreases precipitously after the maximum at  $n=6$ , for  $\text{I}_2^-$  it is the only channel observed for large clusters.

The dramatic difference between the dissociation dynamics of the two systems can be qualitatively understood by comparing the structures of the two cluster ions. For  $\text{I}_2^-$ , the first solvent molecules pack around the waist of the ionic core. In the asymmetric  $\text{ICl}^-$  molecule, the solvent molecules will first solvate the smaller Cl end of the ion. The difference in ionic radii drastically changes the  $\text{ICl}^-$  cluster

structure and this structural difference plays a major role in the very different caging efficiencies for the small clusters.

The minimum energy structures for  $\text{ICl}^-(\text{CO}_2)_4$  and  $\text{ICl}^-(\text{CO}_2)_8$  have been calculated by Faeder and co-workers<sup>29</sup> using Monte Carlo simulations and are shown in Fig. 7. These calculations included the  $\text{ICl}^-$  ground state potential energy surface and electrostatic interactions between the  $\text{ICl}^-$ - $\text{CO}_2$  and the  $\text{CO}_2$ - $\text{CO}_2$  molecules. These interactions are described as the sum of Lennard-Jones (6-12) potential terms and Coulombic interactions between point charges. The electronic polarizability of the  $\text{CO}_2$  solvent (e.g., ion-induced dipole interaction) is neglected. These calculations predict a preferential packing of the  $\text{CO}_2$  molecules around the smaller, more electronegative Cl atom, and this arrangement of solvent molecules further polarizes the slightly asymmetric charge distribution initially present in the bare ion. This effect is due primarily to the smaller size of the Cl atom, the slight asymmetry in the initial charge distribution being less important. Five or six  $\text{CO}_2$  molecules completely enclose the Cl end of the ion, producing a strong electric field component along the bond axis.

In contrast, Monte Carlo simulations of  $\text{I}_2^-(\text{CO}_2)_n$  predict that the first four  $\text{CO}_2$  molecules pack around the center of mass of the ionic core.<sup>15,58</sup> Experimental observations are consistent with this view, and solvation around the center-of-mass does not appear to induce caging of the dissociating molecule. In order to effectively “cage” the products, it is necessary that the solvent molecules be positioned near the end of the ion. The Monte Carlo calculations show that the next  $\text{CO}_2$  molecules solvate the same end of the  $\text{I}_2^-$  core, producing “half solvated”  $\text{I}_2^-(\text{CO}_2)_n$  clusters for  $n=8$  and 9. Preferential solvation of one end is a consequence of the unusually strong  $\text{CO}_2$ - $\text{CO}_2$  bond, which is comparable to that for  $\text{I}^-$ - $\text{CO}_2$ . In addition, simulations by Papanikolas and co-workers,<sup>58,59</sup> for which the polarization of the solvent molecules was not included, show that this asymmetric packing produces a sufficiently strong ( $\sim 10^6$  V/cm) electric field at the  $\text{I}_2^-$  end to significantly polarize the charge distribution on the solute, leading to more solvation of one end of the cluster.

Another way to understand the difference between the dissociation dynamics of  $\text{ICl}^-$  and  $\text{I}_2^-$  is to look at the kinematics. Upon dissociation, the heavy I atom is relatively stationary, with the lighter Cl fragment carrying away  $\sim 3/4$  of the kinetic energy released at a corresponding much higher velocity. The Cl end is surrounded by solvent molecules with roughly the same mass, providing an efficient energy transfer partner, and thereby enhancing recombination. Neither this asymmetric structure nor the solvent mass match are present in  $\text{I}_2^-$  clusters, reducing the caging efficiency compared with the  $\text{ICl}^-$  for small cluster sizes. Unit caging efficiency for  $\text{ICl}^-$  is not observed as the solvated  $\text{Cl}^-$  becomes a more accessible product channel.

In a simplified picture, recombination of the dissociating diatomic molecule can occur by two distinct mechanisms. In the first mechanism, recombination can occur due to the attraction of the nascent ion  $\text{I}^-$  (or  $\text{Cl}^-$ ) or atom to the solvent molecules. In the second, recombination occurs because of

repulsive interactions with the hard sphere walls of the solvent cage.

From the Monte Carlo  $\text{ICl}^-(\text{CO}_2)_n$  structures and the measured caging efficiency, we conclude that recombination in these cluster ions is more likely to occur via the latter mechanism, by which the dissociating molecule is caged by the “billiard ball” interaction with the solvent molecules. On the other hand, for  $\text{I}_2^-$  clusters both mechanisms are important. For smaller  $\text{I}_2^-$  cluster ions, a combination of both mechanisms leads to recombination of the dissociating diatomic molecule, because only one end of the ionic chromophore is capped. In the larger clusters, recombination is more likely to occur by the latter mechanism.<sup>60</sup>

### 3. Caging efficiency as a function of excitation energy

As shown in Fig. 8, we observe  $\text{ICl}^-$  caging with even one solvent molecule. After recombination, the deposited energy becomes available for evaporation of the solvent molecules. Loss of one solvent molecule is not sufficient to dissipate all of the available energy, and substantial vibrational excitation of the recombined ion is likely. This is supported by the fact that the only detected caged fragment for  $\text{ICl}^-(\text{CO}_2)_n$ , for  $n \leq 4$ , was bare  $\text{ICl}^-$ . Also, the mass match between the Cl atom and the  $\text{CO}_2$  facilitates efficient energy transfer to the departing monomer. This mass match could account for the small number of solvent molecules lost by evaporation as the diatomic molecule recombines.

As the dissociating molecule recombines and undergoes vibrational relaxation, the excitation energy becomes available for evaporation of  $\text{CO}_2$  monomers. The total number of  $\text{CO}_2$  molecules lost depends upon the excitation energy, the binding energy,  $D_0$ , of the  $\text{CO}_2$  to the cluster, and the kinetic energy of the departing monomer. An upper limit to the  $D_0$  of a given solvent molecule to the ionic core can be estimated by determining the average number of  $\text{CO}_2$  molecules lost after recombination and vibrational relaxation and then dividing the excitation energy by that number. Papanikolas *et al.*<sup>15</sup> used this procedure to calculate an upper limit of 250 meV for a  $\text{CO}_2$  molecule bound to  $\text{I}_2^-$ . Of this amount, approximately 50 meV is the kinetic energy partitioned to the  $\text{CO}_2$  molecule during the evaporation process. Following the same procedure, we estimated the upper limit to the binding energy of  $\text{CO}_2$  to  $\text{ICl}^-$ . With 644 nm excitation, the amount of energy deposited into the cluster is 1.93 eV, which places an upper bound on the  $D_0$  of  $\text{CO}_2$  to the cluster of about 340 meV. At 740 nm,  $D_0$  was also found to be 340 meV. The uncertainty in the binding energy is estimated to be 50 meV. Further experiments on larger clusters, where all the photon energy can be dissipated through evaporation, will be required to improve the uncertainty of this measurement.

The  $\text{CO}_2$ - $\text{ICl}^-$  binding energy varies quite substantially according to the position of the solvent molecule with respect to the ionic core. The solvent molecules near the Cl end will be bound more strongly than those near the iodine end. The difference in the  $\text{CO}_2$  binding energy for  $\text{ICl}^-$  and  $\text{I}_2^-$  is about 90 meV, being higher for  $\text{ICl}^-$ . This result suggests that the first  $\text{CO}_2$  molecules solvate the Cl end. Keesee

*et al.*<sup>61</sup> used high-pressure mass spectrometry to determine a binding enthalpy at 298 K for  $\text{I}^-$  and  $\text{Cl}^-$  to a  $\text{CO}_2$  molecule. These binding enthalpies so obtained are  $\Delta H_{0,1}^0(\text{Cl}^- - \text{CO}_2) = (0.347 \pm 0.004)$  eV and  $\Delta H_{0,1}^0(\text{I}^- - \text{CO}_2) = (0.243 \pm 0.004)$  eV. The  $\Delta H^0$  at 298 K can be converted to  $D_0$  using the vibrational frequencies of the clusters. Assuming that all of the anion complexes intramolecular vibrational frequencies are approximately the same as that measured by Zhao and co-workers<sup>62</sup> for the stretch in  $\text{I}^-(\text{CO}_2)$ ,  $64 \text{ cm}^{-1}$ , we can estimate  $D_0$  for  $\text{Cl}^- - \text{CO}_2$  and  $\text{I}^- - \text{CO}_2$  to be 0.358 and 0.254 eV, respectively, consistent with our results.

## V. CONCLUSIONS

Photodissociation of  $\text{ICl}^-(\text{CO}_2)_n$  ( $n \leq 8$ ) cluster ions at 644 and 740 nm has been carried out using a tandem time-of-flight mass spectrometer. The photofragment ions are mass analyzed in a secondary TOF that consists of a single field reflectron. At these wavelengths, the only channel open for bare  $\text{ICl}^-$  is photodissociation to produce  $\text{I}^- + \text{Cl}$ . Cluster photofragmentation studies find that for small clusters,  $n \leq 2$ , the  $\text{I}^-$  direct photoproduct is the dominant channel, as for bare  $\text{ICl}^-$ . For ions with more than two  $\text{CO}_2$  molecules, both  $\text{Cl}^-$  and  $\text{ICl}^-$  based photofragment channels also appear, indicating that charge transfer has been mediated by the solvent. The mechanism for this nonadiabatic transition to the ground state involves strong coupling with the solvent molecules. The initial caging of the dissociating ionic core is more efficient for  $\text{ICl}^-(\text{CO}_2)_n$  cluster ions than for  $\text{I}_2^-(\text{CO}_2)_n$  ions, but the  $\text{ICl}^-$  based products rapidly decrease for the larger clusters and are replaced by the  $\text{Cl}^-$  based products. We present several possible explanations for these findings that depend on the intracluster attractive forces and the efficiency of energy transfer from the ion core to the solvent. We find that solvation dramatically affects the outcome of the photodissociation reaction. Spectroscopic measurements on  $\text{ICl}^-(\text{CO}_2)_4$  show that the solvent molecules do not strongly affect the electronic structure of  $\text{ICl}^-$  near the equilibrium bond length. The effects we observe result from dynamical interactions with the solvent, not static solvent-induced shifts in the electronic structure.

Future experiments will investigate the role of the solvent molecules in larger cluster ions. Finally, pump-probe experiments using a femtosecond laser system will probe the dynamics for solvent reorganization around the newly formed ion.

## ACKNOWLEDGMENTS

The authors wish to thank James Faeder, Dr. Paul Maslen, and Dr. Robert Parson for their theoretical work on  $\text{ICl}^-$  and  $\text{ICl}^-(\text{CO}_2)_n$  cluster ions. Further thanks are given to Dr. John M. Papanikolas and Dr. Paul J. Campagnola for helpful discussions during the course of this investigation. We would also like to thank Dr. Stephen R. Leone, Dr. Mary K. Gilles, and Dr. Paul Wenthold for proofreading the manuscript. Support by the National Science Foundation Grants PHY 90-12244, CHE 93-18639, and AFOSR is gratefully acknowledged.

- <sup>1</sup>S. Goyal, D. L. Schutt, and G. Scoles, *Acc. Chem. Res.* **26**, 123 (1993).
- <sup>2</sup>A. McIlroy, R. Lascola, C. M. Lovejoy, and D. J. Nesbitt, *J. Phys. Chem.* **95**, 2636 (1991).
- <sup>3</sup>P. A. Block, L. G. Pedersen, and R. E. Miller, *J. Chem. Phys.* **98**, 3754 (1993).
- <sup>4</sup>R. J. Saykally and G. A. Blake, *Science* **259**, 1570 (1993).
- <sup>5</sup>D. J. Donaldson and V. Vaida, *J. Chem. Phys.* **87**, 2522 (1987).
- <sup>6</sup>J. M. Skene, J. C. Drobits, and M. I. Lester, *J. Chem. Phys.* **85**, 2329 (1986).
- <sup>7</sup>R. Knochenmuss and S. Leutwyler, *J. Chem. Phys.* **91**, 1268 (1989).
- <sup>8</sup>R. Knochenmuss and D. Ray, *Chem. Phys. Lett.* **215**, 188 (1993).
- <sup>9</sup>O. Echt, P. D. Dao, S. Morgan, and A. W. Castleman, Jr., *J. Chem. Phys.* **82**, 4076 (1985).
- <sup>10</sup>S. I. Ionov, G. A. Brucker, C. Jaques, L. Valachovic, and C. Wittig, *J. Chem. Phys.* **97**, 9486 (1992).
- <sup>11</sup>M. F. Hineman, G. A. Brucker, D. F. Kelley, and E. R. Bernstein, *J. Chem. Phys.* **97**, 3341 (1992).
- <sup>12</sup>J. Steadman and J. A. Syage, *J. Chem. Phys.* **92**, 4630 (1990).
- <sup>13</sup>J. J. Breen, L. W. Peng, D. M. Willberg, A. Heikal, P. Cong, and A. H. Zewail, *J. Chem. Phys.* **92**, 805 (1990).
- <sup>14</sup>M. L. Alexander, N. E. Levinger, M. A. Johnson, D. Ray, and W. C. Lineberger, *J. Chem. Phys.* **88**, 6200 (1988).
- <sup>15</sup>J. M. Papanikolas, J. R. Gord, N. E. Levinger, D. Ray, V. Vorsa, and W. C. Lineberger, *J. Phys. Chem.* **95**, 8028 (1991).
- <sup>16</sup>J. M. Papanikolas, V. Vorsa, M. E. Nadal, P. J. Campagnola, H. K. Buchenau, and W. C. Lineberger, *J. Chem. Phys.* **99**, 8733 (1993).
- <sup>17</sup>J. M. Papanikolas, P. J. Campagnola, V. Vorsa, M. E. Nadal, H. K. Buchenau, R. Parson, and W. C. Lineberger, in *The Chemical Dynamics and Kinetics of Small Radicals*, edited by K. Liu and A. Wagner (World Scientific, Singapore, 1995).
- <sup>18</sup>E. Rabinowitch and W. C. Wood, *Trans. Faraday Soc.* **32**, 1381 (1936).
- <sup>19</sup>J. H. Choi, K. T. Kumata, B. M. Haas, Y. Cao, M. S. Johnson, and M. Okumura, *J. Chem. Phys.* **100**, 7153 (1994).
- <sup>20</sup>J. M. Farrar, in *Current Topics in Ion Chemistry and Physics*, edited by C. Y. Ng and I. Powis (Wiley, New York, 1992).
- <sup>21</sup>T. D. Märk and A. W. Castleman, Jr., in *Advances in Atomic and Molecular Physics* (Academic, New York, 1985), Vol. 20.
- <sup>22</sup>D. W. Arnold, S. E. Bradforth, E. H. Kim, and D. M. Neumark, *J. Chem. Phys.* **97**, 9468 (1992).
- <sup>23</sup>D. W. Arnold, S. E. Bradforth, E. H. Kim, and D. M. Neumark, *J. Chem. Phys.* **102**, 3510 (1995).
- <sup>24</sup>T. J. Selegue, O. M. Cabarcos, and J. M. Lisy, *J. Chem. Phys.* **100**, 4790 (1994).
- <sup>25</sup>L. N. Ding, M. A. Young, P. D. Kleiber, and W. C. Stwalley, *Chem. Phys. Lett.* **212**, 499 (1993).
- <sup>26</sup>P. J. Campagnola, D. J. Lavrich, M. J. DeLuca, and M. A. Johnson, *J. Chem. Phys.* **94**, 5240 (1991).
- <sup>27</sup>S. G. Donnelly and J. M. Farrar, *J. Chem. Phys.* **98**, 5450 (1993).
- <sup>28</sup>W. C. Lineberger, M. E. Nadal, P. J. Campagnola, V. Vorsa, P. D. Kleiber, J. M. Papanikolas, P. E. Maslen, J. Faeder, R. Parson, and O. Poplawski, Proceedings of the Robert A. Welch Foundation 38th Conference on Chemical Research, Houston, TX, October 24–25, 1994, pp. 174–184.
- <sup>29</sup>J. Faeder, P. Maslen, and R. Parson (private communication).
- <sup>30</sup>R. A. Marcus, *J. Chem. Phys.* **24**, 966 (1956); R. A. Marcus, *J. Chem. Phys.* **24**, 979 (1956); R. A. Marcus, *J. Chem. Phys.* **26**, 867 (1957).
- <sup>31</sup>M. D. Newton and N. Sutin, *Ann. Rev. Phys. Chem.* **35**, 437 (1984).
- <sup>32</sup>W.-S. Sheu and P. J. Rossky, *Chem. Phys. Lett.* **202**, 186 (1993).
- <sup>33</sup>W. P. Keirstead, K. Wilson, and J. T. Hynes, *J. Chem. Phys.* **95**, 5256 (1991).
- <sup>34</sup>M. J. DeLuca, C. C. Han, and M. A. Johnson, *J. Chem. Phys.* **93**, 268 (1990).
- <sup>35</sup>P. Y. Cheng, D. Zhong, and A. H. Zewail, *Chem. Phys. Lett.* **242**, 369 (1995).
- <sup>36</sup>H.-S. Kim, C.-H. Kuo, and M. T. Bowers, *J. Chem. Phys.* **87**, 2667 (1987); H.-S. Kim, C.-H. Kuo, and M. T. Bowers, *J. Chem. Phys.* **88**, 4557 (1988).
- <sup>37</sup>R. A. Beyer and J. A. Vanderhoff, *J. Chem. Phys.* **65**, 2313 (1976).
- <sup>38</sup>M. H. Shen and J. M. Farrar, *J. Phys. Chem.* **93**, 4386 (1989).
- <sup>39</sup>M. J. Blandamer and M. F. Fox, *Chem. Rev.* **70**, 59 (1970).
- <sup>40</sup>P. F. Barbara, G. C. Walker, and T. P. Smith, *Science* **256**, 975 (1992).
- <sup>41</sup>M. Maroncelli, J. MacInns, and G. R. Fleming, *Science* **243**, 1674 (1989).
- <sup>42</sup>M. A. Johnson and W. C. Lineberger, in *Techniques for the Study of Ion*

- Molecule Reactions*, edited by J. M. Farrar and W. Saunders, Jr. (Wiley, New York, 1988).
- <sup>43</sup>N. E. Levinger, Ph.D. thesis, University of Colorado at Boulder, 1990.
- <sup>44</sup>M. L. Alexander, N. E. Levinger, M. A. Johnson, D. Ray, and W. C. Lineberger, *J. Chem. Phys.* **88**, 6200 (1988).
- <sup>45</sup>N. E. Levinger, D. Ray, M. L. Alexander, and W. C. Lineberger, *J. Chem. Phys.* **89**, 5654 (1988).
- <sup>46</sup>N. E. Levinger, D. Ray, K. K. Murray, A. S. Mullin, C. P. Schulz, and W. C. Lineberger, *J. Chem. Phys.* **89**, 71 (1988).
- <sup>47</sup>M. E. Nadal, P. D. Kleiber, and W. C. Lineberger (in preparation).
- <sup>48</sup>C. E. Moore, in *Atomic Energy Levels* (National Bureau of Standards, Washington DC, 1949).
- <sup>49</sup>L. Bañares and A. G. Ureña, *Chem. Phys. Lett.* **176**, 178 (1991).
- <sup>50</sup>R. C. Weast, *CRC Handbook of Chemistry and Physics* (CRC, Fl, 1985), p. F-164.
- <sup>51</sup>R. N. Compton and P. W. Reinhardt, *J. Chem. Phys.* **63**, 3821 (1975).
- <sup>52</sup>M. J. DeLuca, B. H. Niu, and M. A. Johnson, *J. Chem. Phys.* **88**, 5857 (1988).
- <sup>53</sup>Y. Marcus, *Ion Solvation* (Wiley, New York, 1985), pp. 41–44, 105–133.
- <sup>54</sup>Y. Lin, R. C. Dorfman, and M. D. Fayer, *J. Chem. Phys.* **93**, 3550 (1990).
- <sup>55</sup>M. D. Fayer, L. Song, S. F. Swallen, R. C. Dorfman, and K. Weidemaier, in *Ultrafast Dynamics of Chemical Systems*, edited by J. D. Simon (Kluwer Academic, Dordrecht, the Netherlands, 1994), pp. 37–80.
- <sup>56</sup>J. Mattay and M. Vondenhof, *Topics Curr. Chem.* **159**, 219 (1991).
- <sup>57</sup>G. Ciccotti, M. Ferrario, J. T. Hynes, and R. Kapral, *J. Chem. Phys.* **93**, 7137 (1990).
- <sup>58</sup>J. M. Papanikolas Ph. D. Thesis, University of Colorado at Boulder (May 1994).
- <sup>59</sup>J. M. Papanikolas, P. E. Maslen, and R. Parson, *J. Chem. Phys.* **102**, 2452 (1995).
- <sup>60</sup>F. G. Amar and B. J. Berne, *J. Phys. Chem.* **88**, 6720 (1984).
- <sup>61</sup>R. G. Keesee, N. Lee, and A. W. Castleman, Jr., *J. Chem. Phys.* **73**, 2195 (1980).
- <sup>62</sup>Y. Zhao, C. C. Arnold, and D. M. Neumark, *J. Chem. Soc. Faraday Trans. 2* **89**, 1449 (1993).